THE ROTATIONAL VIBRATIONAL SPECTRUM OF MONOCHLOROACETYLENE

by

CONNOR FITZPATRICK WILLEMSEN

A THESIS

Presented to the Department of Chemistry
and the Robert D. Clark Honors College
in partial fulfillment of the requirements for the degree of
Bachelor of Science

June 2016

An Abstract of the Thesis of

Connor Fitzpatrick Willemsen for the degree of Bachelor of Science
in the Department of Chemistry to be taken June 2016

Title: THE ROTATIONAL VIBRATIONAL SPECTRUM OF MONOCHLOROACETYLENE

Approved: John Hardwick

John Hardwick

The $2\nu_1$ bands for $HCC^{35}Cl$ and $HCC^{37}Cl$, the $\nu_1+\nu_2+2\nu_4$ band for $HCC^{35}Cl$, and the $(\nu_1+\nu_4)^1$-ν_4^1 hot band for $HCC^{35}Cl$ have been measured between 6370 and 6660 cm^{-1} using a custom spectrometer based around an external cavity diode laser. Upper and lower state *J*-values have been assigned to each spectral line measured and confirmed via mathematical modeling of the spectra. A double perturbation was identified and characterized in $2\nu_1$ band of $HCC^{37}Cl$ and *l*-type doubling was identified and characterized in the $(\nu_1+\nu_4)^1$-ν_4^1 hot band of $HCC^{35}Cl$. Rotational and centrifugal distortion coefficients were calculated for all bands, along with additional constants to characterize the perturbed states and the *l*-type doubling. Modeling using a Voigt line shape was used to subtract the peaks of the $HCC^{35}Cl$ main band to allow more complete analysis of the $HCC^{37}Cl$ main band and a novel fast-Fourier transform-based method was used for baseline correction. Assignment accuracy of unblended lines for the various bands ranges from 2.5×10^{-4} cm^{-1} to 1.8×10^{-3} cm^{-1}.

Acknowledgements

My sincerest thanks go to Dr. John Hardwick, who not only gave countless hours and untold effort to this project, but who also inspired my initial interest in physical chemistry through his fascinating Physical Chemistry Laboratory course. The depth of understanding that I have gained in the past year of research would not be possible without his remarkable patience and perseverance in helping me and answering my questions. He has also contributed a tremendous amount of work to this project, writing computer programs and helping with data analysis.

Thanks are also due to Professor David Tyler and Dr. Robert Hubbard for their roles as my first research mentors. Many of the skills and lessons they taught me have invaluably helped with the research herein.

My parents have provided immeasurable support both through the process of writing this thesis and through my entire college experience. For their contribution, no amount of thanks is sufficient.

Table of Contents

Background

Newtonian physics treats energy as existing as a continuous function, in other words, an object may possess any amount of energy whether that amount is very small or very large. For examining the behavior of macroscopic objects such as an apple dropping from a tree or a plane flying through the sky this model works very well. However, on the molecular and particle level, energy is not continuous but rather discrete. The energy levels at which a particular molecule may exist are not smooth and continuous like a ramp, but rather take particular and specific values. This is very much analogous to standing on a set of stairs. It is possible to stand on any one particular step, and to move between steps, but it is not possible to stand in between two of the steps.

The ability of molecules to only take on discrete energy levels is called quantization, and is a fundamental concept of quantum physics. Each way in which a molecule's energy may be defined has its own set of quantum energy levels: rotational, or how the molecule rotates about its center of mass; vibrational, or how the molecule stretches and bends; translational, or movement through three dimensional space; and electronic, or the nature of the excitation of the electrons of a molecule. The first two of these, rotational and vibrational energy levels, form the theoretical basis for the type of spectroscopy used herein.

If the energy levels at which a molecule can exist have specific, quantized values, then there are also specific differences in values between these states. A common demonstration in general chemistry courses involves using a prism to separate the light emitted by electronically excited hydrogen gas. Four visible colors of light are seen and each color corresponds to photons that posses a level of energy equivalent to

the difference in energy between one of four excited states and the ground state, which can be thought of as a baseline or resting condition. Figure 1 depicts transitions between rotational states, denoted by *J*, and vibrational states, denoted by *v*.

By convention, *J*' is used to refer to the rotational quantum number of the upper, or final state, and *J*'' is used to refer to the rotational quantum number of the lower, or initial state, with respect to a given energy transition. This convention is also used to denote the constants which describe the behavior of the band, for example *B*'' is the rotational constant of the lower state.

Figure 1: Rotational-vibrational energy transitions.

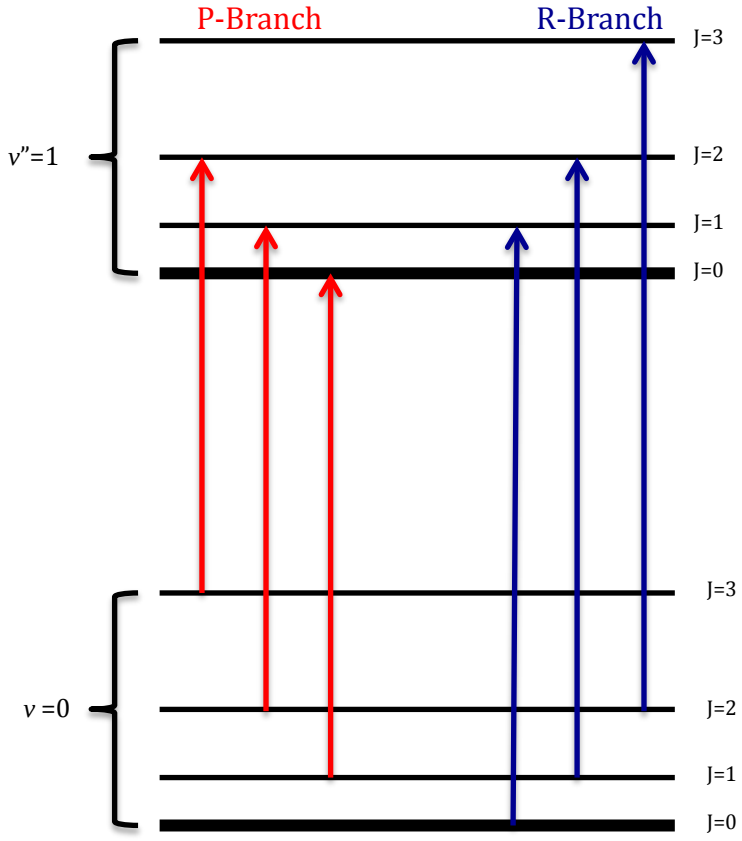

Rotational-vibrational spectroscopy observes differences in energy between the ground state and various quantum rotational and vibrational energy states. For our experiment a tunable diode laser is used to generate a laser beam that smoothly sweeps through a wide range of frequencies, thereby changing the amount of energy in the photons of the beam. The laser beam is passed through a gaseous sample and the photons of various energies in the beam cause the molecules in the sample to

reach various excited quantum rotational and vibrational states. When a photon in the beam causes a molecule to become excited, that photon is absorbed and the intensity of the beam is reduced. The resulting modulation of the intensity of the beam during the sweep of the laser is detected by a sensor and electronically logged, along with a precise timing signal.

A secondary path of the swept laser passes through an interferometer, which uses precisely spaced mirrors to exploit phase cancellation in the laser beam to produce an interferogram, or a graph that gives very precisely spaced peaks when plotted as a function of time. This is analogous to having a ruler with evenly spaced markers but no numbers; you can figure out the distance between any two points but not an absolute location. A third beam passes through a sample of acetylene, a reference compound for which the location of the spectral peaks is known to within an error of one part in ten trillion and for which we used the precise line determinations of Madej *et al*. The location of these peaks provides the absolute scale lacked by the interferogram and when computationally combined the two are capable of generating an accurate measurement of the wavelength at which the laser was operating at any given point during the measurement. This is critically important, since the detectors used on the laser beams are only capable of measuring intensity, not wavelength.

The intensity information from the sample beam and the wavelength information from the interferogram and acetylene reference are computationally combined to create a spectrum that graphically shows sharp peaks at frequencies at which the sample molecules absorbed more or less light. The spacing between various peaks corresponds

to the difference in quantum energy levels between the ground state and various excited rotational and vibrational states.

Figure 2 shows the five fundamental vibrational modes of monochloroacetylene, denoted v_1 through v_5. Each vibrational mode has an associated fundamental transition as reported by Hore *et al.*, but which fall outside the frequency range of our spectrometer. However, we are able to detect transitions which involve combinations of these vibrational modes as well as their associated rotational energy states. v_1 is the C-H stretch, v_2 is the C≡C stretch, v_3 is the C-Cl stretch, v_4 is the H-C≡C deformation, and v_5 is the C≡C-Cl deformation.

Figure 2: The fundamental vibrational modes of monochloroacetylene.

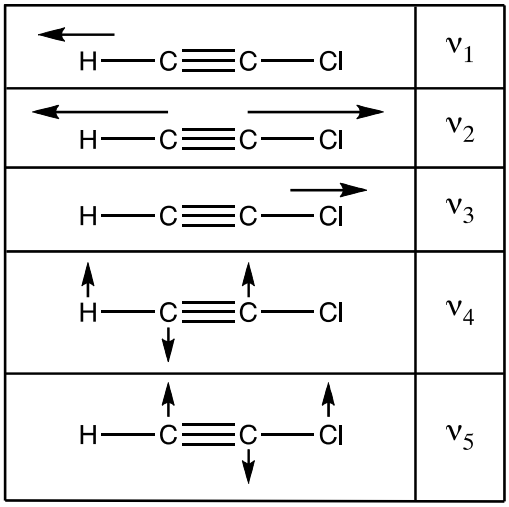

We use notation involving the various v_n vibrational modes to denote specific bands. Cold bands involve a vibrational transition between the ground state and an excited vibrational state, which may or may not involve multiple vibrational modes, along with rotational transitions. Hot bands involve a vibrational transition between two different excited vibrational states, each of which may or may not involve multiple vibrational modes, along with rotational transitions.

Cold bands are denoted by writing the number of quanta of energy in each vibrational mode before the mode and using plus symbols to indicate a band that involves multiple vibrational modes. For example, the $2v_1$ band involves a transition between the vibrational ground state and the vibrational state that has two quanta in the

v_1 vibrational mode, along with associated rotational transitions. The $v_1+v_2+2v_4$ band involves a transition between the ground state and a state with one quantum in the v_1 vibrational mode, one quantum in the v_2 vibrational mode, and two quanta in the $2v_4$ vibrational mode.

Hot bands are detonated by writing the notation as described for cold bands for each of the vibrational states involved, placing each state's notation in parenthesis, and using a minus sign between them. Superscripts may indicate the value of *l*, the vibrational angular momentum quantum number associated with two-dimensional bending modes. Therefore the $(v_1+v_4)^1$-v_4^1 hot band involves a transition between an excited vibrational state with one quantum of energy in the v_1 vibrational mode and one quantum of energy in the v_4 vibrational mode and another excited vibrational state with one quantum of energy in the v_4 vibrational mode, as well as the associated rotational transitions. The superscripts indicate that l=1 for both states, which is also referred to as a π-state.

As shown in Figure 1, rotational energy states are typically much more closely spaced than vibrational energy states. Therefore we define bands as the combination between a single vibrational transition and many rotational transitions, where the center, or origin, of the band is defined by the vibrational transition and the spread of peaks outward from the center of the band is defined the by value of the rotational quantum number, *J*, for each peak.

The frequency of absorbance peaks observed depends directly on the difference in energy of the quantum states involved. Accordingly we can use previous work that observed transitions between some of the same states to infer differences between our

absorbance frequencies. In particular, we can combine microwave spectral data that examine smaller energy transitions with certain transitions that we detect to infer the energy of larger transitions. This is referred to as the method of combination differences and is useful because it does not depend on mathematical modeling but rather on the conservation of energy of the transitions between various states.

Nela *et al*. have examined the spectrum of monochloroacetylene using both photoacoustic and infrared laser spectroscopy, the later similar to our technique and operating between 4,000 and 10,000 cm^{-1}, and have provided extensive analysis of both rotational and vibrational states along with transition assignments and physical constants. Hore, *et al.* have also used infrared laser rotational vibrational spectroscopy to characterize monochloroacetylene, but across a different wavenumber spectrum from our or the work of Nela *et al*. Their work is invaluable, along with the work of Nela *et al.*, to provide physical constants to confirm our calculations and transition assignments through the method of combination differences.

Note that two distinct forms of monochloroacetylene are present as chlorine is predominantly composed of two isotopes. The lighter isotope, ^{35}Cl, comprises approximately 76% of all naturally occurring chlorine, while the heavier isotope, ^{37}Cl, comprises approximately 24% of all naturally occurring chlorine. The difference in the weights of the chlorine isotopes leads to distinct spectra for each form of monochloroacetylene, one containing ^{37}Cl and the other containing ^{35}Cl, which occur with abundances proportional to the abundances of their respective isotopes in nature. The absorbances of the bands of each isotopologue are also roughly proportional to

their abundances. Therefore the bands of $HCC^{37}Cl$ have a lower absorbance and are more difficult to accurately assign than are the bands of $HCC^{35}Cl$.

Different molecules rotate and vibrate differently and thus have distinct and characteristic patterns of peaks in a rotational-vibrational spectrum. Molecules whose spectra are known may be identified as components of unknown samples. Alternatively, a rotational-vibrational spectrum may be used to learn about the quantum energy states of a molecule under investigation. The data derived from the spectrum may then be mathematically associated with a variety of physical constants of the molecule, such as its bond lengths and bond angles.

Rotational-vibrational spectroscopy and pure rotational spectroscopy can be used to analyze small amounts of gases present in the atmosphere with several key advantages. Rather than sampling a very small portion of atmosphere and transporting it to a laboratory for one-time analysis in an instrument like a mass spectrometer, a laser used for rotational-vibrational spectroscopy can be directed through the atmosphere and reflected back to the spectrometer off a remotely located mirror. This allows the analysis of physically large samples of atmosphere, including in particular locations like the smokestacks of a power plant, where the emissions to be analyzed could be located in between the spectrometer and a mirror. Samples are easily repeated throughout time as the analysis occurs without the need to capture or transport a sample and can as such render valuable data regarding the changes in the concentration of compounds over time.

The combustion of chlorine-containing compounds and polymers has the potential to produce monochloroacetylene which can be released into the atmosphere

from municipal and chemical waste-disposal incinerators. Dougherty and Collazo-Lopez have argued thermodynamically that monochloroacetylene is the most likely carbon-chlorine fragment of the breakdown of polyvinylidene chloride, best known Saran Wrap, at 1000° Celsius. Their experimental work did not detect monochloroacetylene after high temperature incinerations of polyvinylidene chloride, however they analyzed the gaseous products of their experiment by performing extractions of the contents of liquid nitrogen traps with organic solvents. Considering the highly reactive nature of monochloroacetylene, any amount produced may have reacted before analysis. As rotational-vibrational spectroscopy can detect monochloroacetylene in the gas phase in real time, it may be a superior technique for investigating such emissions. While Saran Wrap is now made of low density polyethylene, which does not contain chlorine, many consumer goods still use polyvinylidene chloride. Chlorinated hydrocarbons and chlorine containing polymers are also ubiquitous in industrial applications.

Methods

Synthesis

Monochloroacetylene was prepared via carbon dioxide-laser pyrolysis of 1,2-dichloroethylene. A stainless steel walled tubular reaction vessel with zinc selenide windows at either end was evacuated of air on a Schlenk line to a pressure of 60 millitorr. A partial pressure of 310 millitorr of 1,2-dichloroethylene was added, followed by a partial pressure of 1.78 torr of sulfur hexafluoride. The sulfur hexafluoride is chemically unreactive and transparent at the frequencies of spectroscopic interest, but efficiently absorbs and converts to heat the energy of the carbon dioxide laser. A 100-watt carbon dioxide laser was used to heat the sample for 180 seconds, after which the pressure in the cooled reaction vessel decreased to 2.7 torr. The gases in the reaction vessel were transferred via Schlenk line to a vacuum-evacuated glass-walled cell for analysis.

Figure 3: Laser pyrolysis of 1,2-dichloroethylene to give monochloroacetylene.

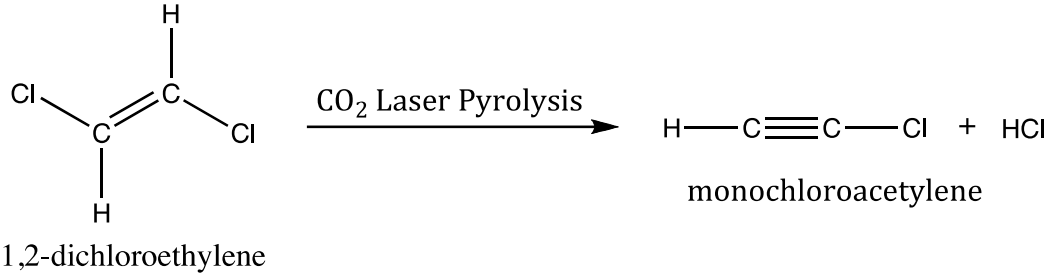

1,2-dichloroethylene

monochloroacetylene

Instrument

A custom infrared rotational-vibrational spectrometer was constructed on a laser table. An infrared New Focus 6428 external cavity diode laser operating between 1500nm and 1570nm offers a relatively smooth and continuous scan through its operating wavelengths due to its Littman-Metcalf design wherein a motorized mirror operates opposite a diffraction grating, changing the angle of incidence upon the diffraction grating and thus the wavelength of the light fed back into the external laser cavity for reinforcement. This selectivity in the wavelength fed back into the external cavity causes only the selected wavelengths to be amplified, allowing operation through a nearly continuous range of frequencies depending on the angle of incidence upon the diffraction grating. The Littman-Metcalf design with its motorized mirror is superior to other external cavity diode lasers with motorized diffraction gratings because it does not change the output direction of the laser beam with frequency, therefore not requiring any compensating mirrors and offering a constant alignment and improved amplitude stability.

The beam is passed through beam splitters to take four different paths to four ThorLabs PDA400 Indium-Gallium-Arsenide amplitude detectors: a reference path directly to a detector, a reference path through a 1-meter path length acetylene sample, a sample path through the monochloroacetylene sample, and a path through an internally coupled Fabry-Perot interferometer with a free spectral range, or separation between adjacent peaks, of 0.009725 cm^{-1}. The Fabry-Perot design's fixed mirrors are capable of providing the very closely and consistently spaced fringes, regardless of the wavelength

of input, that are required to precisely calibrate the spectrum in terms of wavelength when combined with acetylene reference data.

Figure 4 shows the beam paths and setup of the instrument.

The monochloroacetylene sample was contained in a 1-meter long, 1-inch in diameter, glass-walled cell with near-infrared (1550 nm) antireflective coated sodium borosilicate windows.

Figure 4: Instrumental diagram.

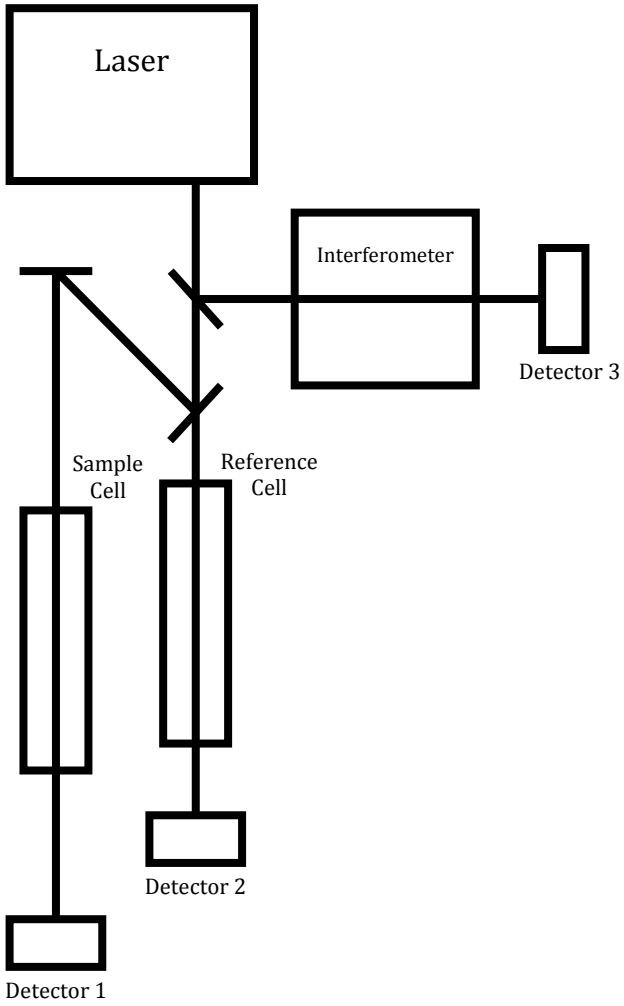

Data Collection

Each detector has a variable gain and offset amplifier that allows both adjustment of the amplitude of the signal and the position of the signal in order to be compatible with the -10v to +10v input range of the National Instruments PCI-6132 analog-to-digital converter set to sample at a rate of 4×10^{-5} seconds per sampling period. The interferometer channel incorporates an op-amp based 1st order high-pass filter to compensate for low frequency oscillations in the laser output.

In order to achieve as much resolution as possible, the analog to digital converter employs discreet conversion circuitry for each channel, with all channels

slaved to a master clock that ensures time-consistent data collection across channels. This allows a substantially higher sampling rate than typical analog to digital converters that multiplex their channels across a single analog to digital circuit, resulting in a sampling rate equivalent to the sampling rate of the converter divided by the number of channels in operation.

Data Processing

Four scans were conducted for each sample. An Igor Pro routine, written by Dr. John Hardwick, converted the time-domain data into the wavenumber-domain by using information from the interferogram and acetylene reference to determine at what wavelength the laser was operating at any given point during the measurement.

The time-domain to wavenumber-domain conversion allows examination of the raw amplitude of the signal received at the sample-path detector as a function of wavenumber. In order to generate an absorbance spectrum that plots how much light the monochloroacetylene sample absorbs at any given wavenumber, the absorptive behavior of how the empty, vacuum evacuated sample cell interacts with the laser beam, or background signal, must be known. This cannot practically be obtained experimentally since infinitesimal alignment changes in the angle of incidence of the laser and sample cell windows affect the background signal significantly. Therefore, the background signal corresponding to an empty sample cell must be computationally deduced from data obtained with the sample present. Further, the background signal is not constant with respect to wavenumber, and thus must be deduced as a nonlinear function of wavenumber. Fundamentally, the spectral data from the sample must be separated from the background signal caused by the interaction of the cell and laser.

The background signal has widely spaced, rounded oscillations whereas the spectral data has closely spaced sharp peaks. Figure 5 shows the wavenumber calibrated signal with the background signal and the spectral peaks. The difference in the shape of the spectral peaks and the background oscillation is exploited by using a fast-Fourier transform (FFT) to transform the spectrum from amplitude in terms of wavenumber to amplitude in terms of time. In the time domain the data corresponding to the closely space peaks of the spectral data occurs after the data corresponding to the widely spaced oscillations of the background noise. Figure 6 shows the results of the fast-Fourier transform. The data points corresponding only to the spectral data may be set to zero and the inverse of the original FFT computed to transform the time domain data back into the wavenumber domain but without any of the spectral peaks, as shown in Figure 7. This gives a well resolved background signal which may be used to obtain the absorbance of light by the sample in terms of wavenumber by taking the quotient of the calibrated amplitude signal and the background signal at each wavenumber data point to give the spectrum in terms of transmittance, as shown in Figure 8. Taking the negative base-ten logarithm of each data point converts the spectrum into absorbance as shown in Figure 9.

Figure 5: Wavenumber calibrated signal with background oscillations and spectral peaks.

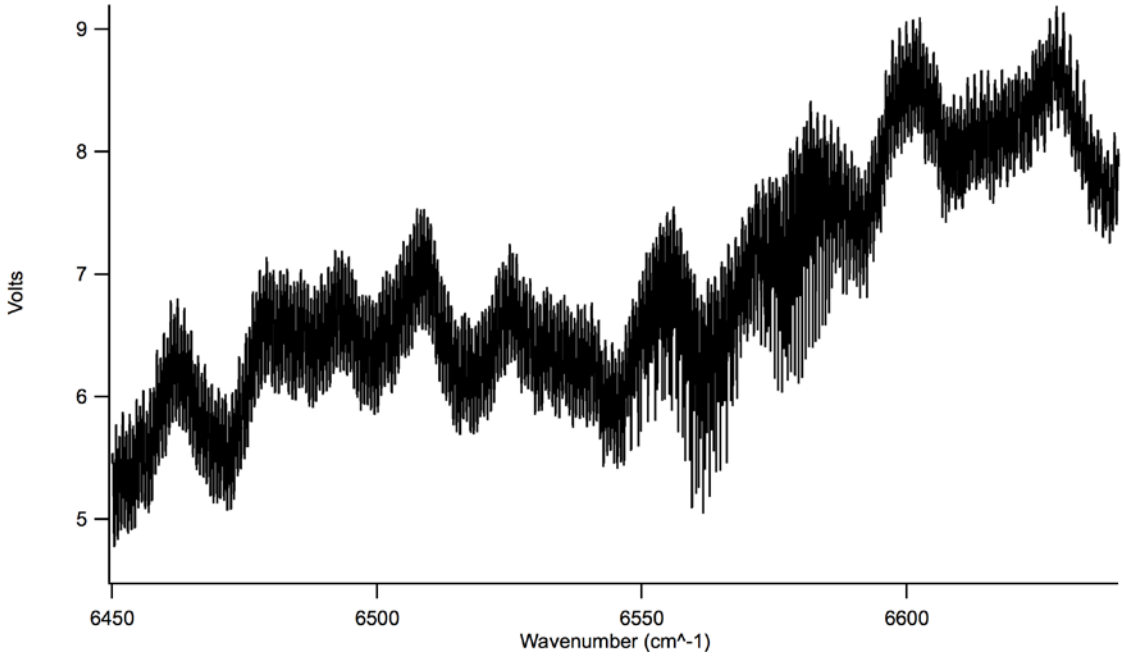

Figure 6: The fast-Fourier transform of Figure 5.

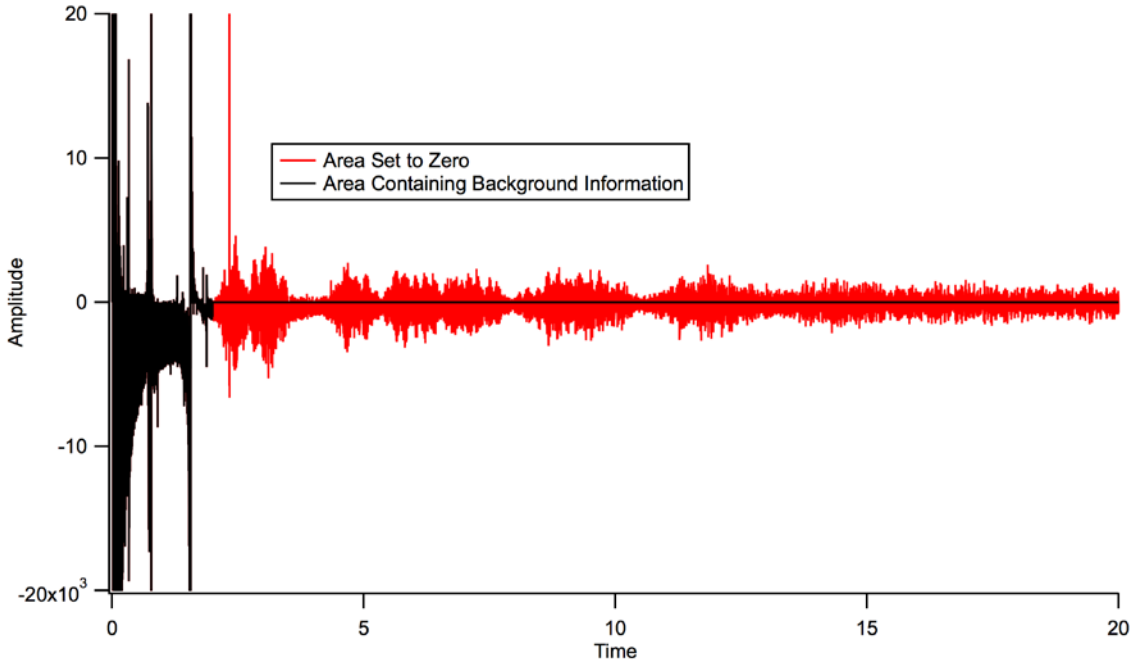

Figure 7: The inverse fast-Fourier transform of the black region in Figure 6.

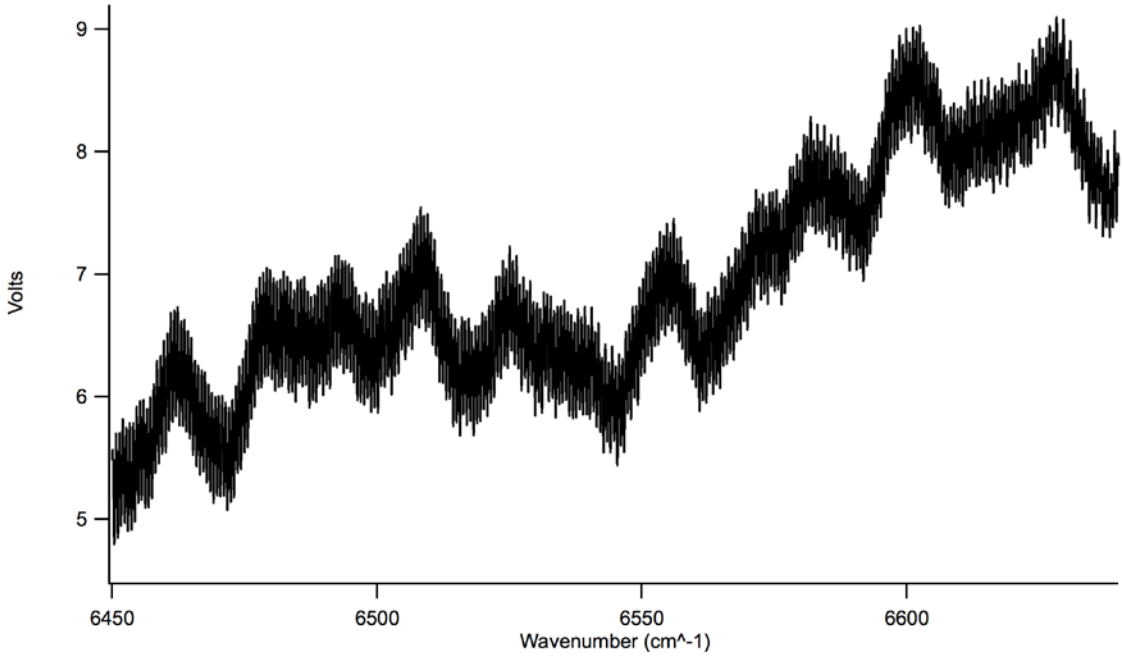

Figure 8: The transmittance spectrum obtained from the point-wise quotient of Figure 7 and Figure 5.

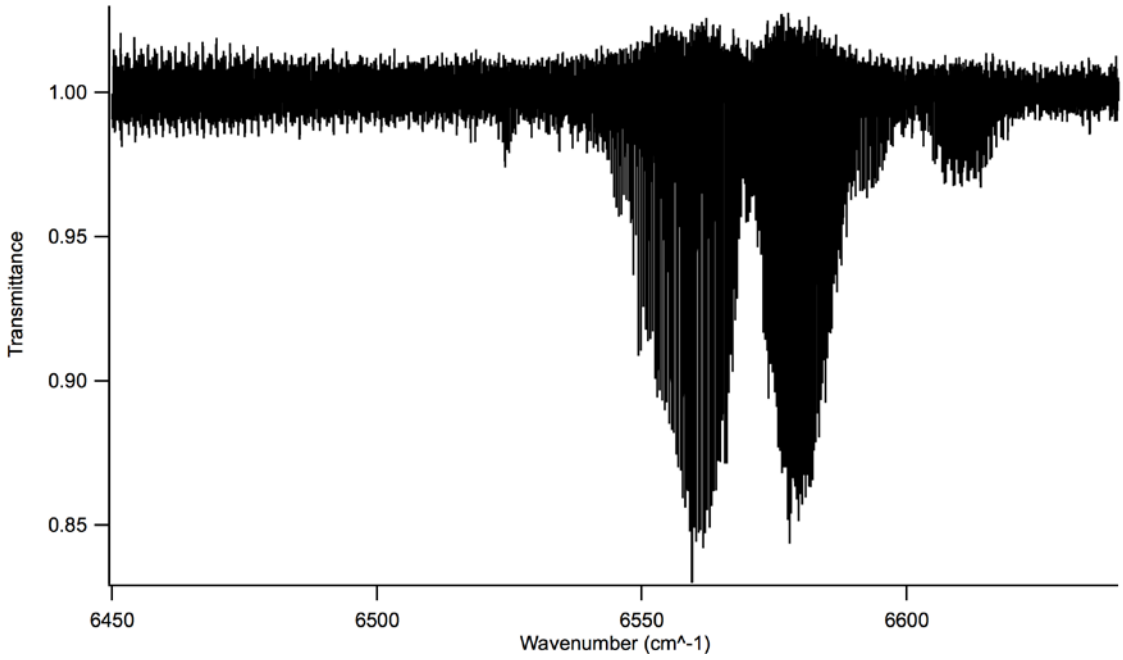

Results and Analysis

Figure 9 shows an overview of the spectrum of monochloroacetylene. The spectrum, in the frequency domain, plots absorbance along the vertical axis and wavenumber along the horizontal axis to allow examination of the nature of the sample's interaction with the laser beam in terms of the wavenumber of the laser light. The wavenumber of the laser light is associated with a specific amount of energy, dependent on the energy of a photon at that wavenumber, and thus allows for determination of the energy of the transitions in rotational and vibration quantum states occurring at that wavenumber. The $2\nu_1$ bands for $HCC^{35}Cl$ and $HCC^{37}Cl$ overlap in the center while the $\nu_1+\nu_2+2\nu_4$ band for $HCC^{35}Cl$ is centered around 6600 cm^{-1} and the $(\nu_1+\nu_4)^1$-$\nu_4{}^1$ hot band is centered around 6530 cm^{-1}.

Figure 9: The absorbance spectrum of monochloroacetylene.

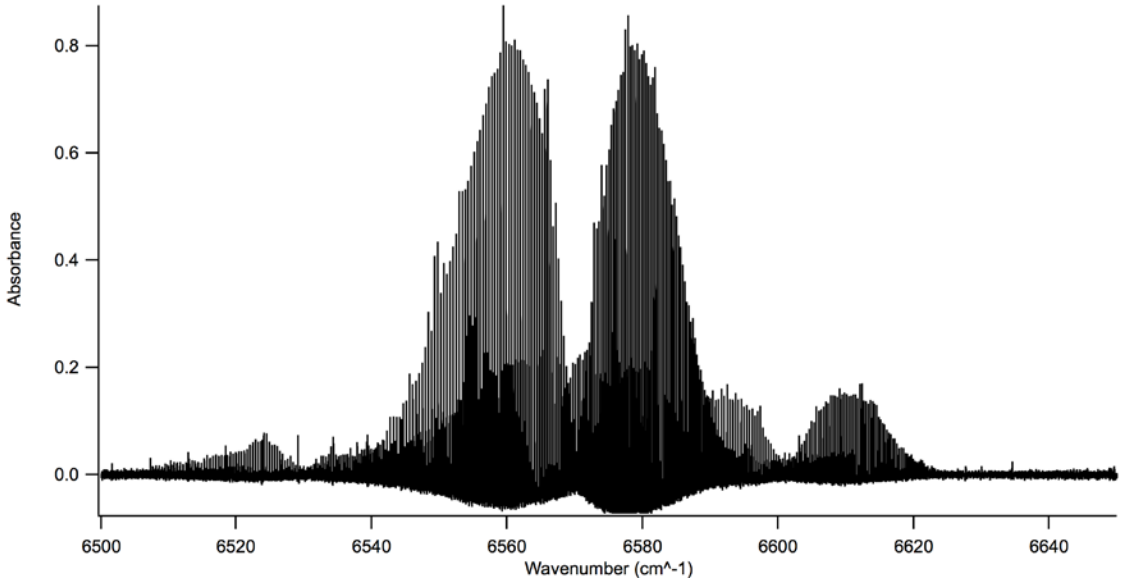

Cold Bands

Three colds bands were characterized, the main $2\nu_1$ bands for $HCC^{35}Cl$ and the $\nu_1+\nu_2+2\nu_4$ band for $HCC^{35}Cl$, all comprised of singlet peaks.

A Voigt profile line-shaping algorithm that is a convolution of Lorentzian and Gaussian line shaping was used in Igor Pro to accurately assign a wavenumber corresponding to the center of each characterized peak. For most of the peaks examined, there was sufficiently little overlap with other peaks to allow accurate assignments. The main bands of $HCC^{35}Cl$ and $HCC^{37}Cl$ have substantial overlap and have different centrifugal distortion coefficients, causing their respective peaks to progressively overlap and then separate across the wavenumber scale. In order to accurately assign the main band of $HCC^{37}Cl$, the Voigt line-shape parameters from the assigned $HCC^{35}Cl$ lines were used reconstruct a model of the $HCC^{35}Cl$ peaks which was then subtracted from the overall spectrum, leaving the $HCC^{37}Cl$ peaks with substantially less overlap and allowing easier and more accurate assignments. Figure 10 shows both the modeled reconstruction of the $HCC^{35}Cl$ peaks and the resultant spectra with clear $HCC^{37}Cl$ peaks after subtraction.

Figure 10: The reconstructed $2\nu_1$ band of $HCC^{35}Cl$, in red, and the result of the subtraction of the former from the overall spectrum, in blue.

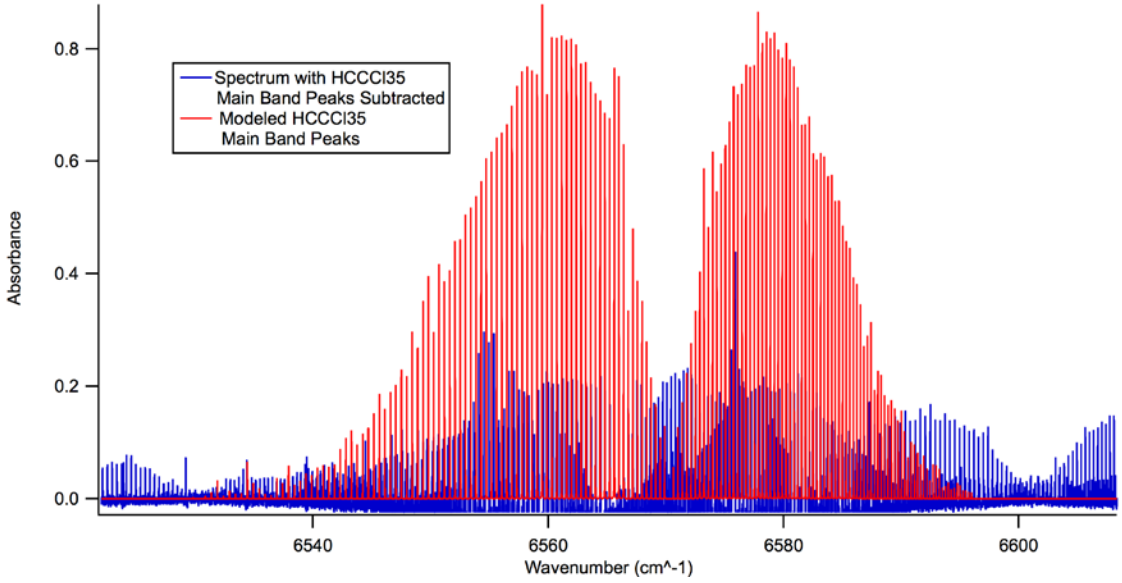

The $2\nu_1$ bands for $HCC^{35}Cl$ and $HCC^{37}Cl$ and the $\nu_1+\nu_2+2\nu_4$ band for $HCC^{35}Cl$ consist of singlet peaks and were modeled in Igor Pro as a function of the rotational quantum numbers J, the rotational constant B_ν, and the centrifugal distortion coefficient D_ν to give the frequency spacing between peaks at J and J+1:

$$\nu_{J+1\leftarrow J} = 2B_\nu(J+1) - 4D_\upsilon(J+1)^3$$

The above equation may be related to the absolute position of any peak, υ, at upper and lower state positions J' and J'', and the band origin, ν_0:

$$\upsilon = [2B_\nu(J'+1) - 4D_\upsilon(J'+1)^3] + \nu_0 - [2B_\nu(J''+1) - 4D_\upsilon(J''+1)^3]$$

A routine in Igor Pro computed values of B_ν, D_ν, and ν_0 from the measured lines and manually assigned J values for each band. The resulting values of the constants were then used to model and reproduce the spectrum, and the original and computed values were compared.

$HCC^{35}Cl$ $2\nu_1$ Band and $\nu_1+\nu_2+2\nu_4$ Band

Accuracy was typically 2.5×10^{-4} cm^{-1} for the $HCC^{35}Cl$ $2\nu_1$ band and 8×10^{-4} cm^{-1} for the $\nu_1+\nu_2+2\nu_4$ band.

Table 1 presents the calculated constants for the $HCC^{35}Cl$ $2\nu_1$ and $\nu_1+\nu_2+2\nu_4$ bands.

Table 1

Calculated constants for $HCC^{35}Cl$ cold bands.

	$2\nu_1$		$\nu_1+\nu_2+2\nu_4$	
Constant	Value	Uncertainty	Value	Uncertainty
ν_0	6570.3	8.80E-05	6601.27	0.00022957
B'	0.18879	1.35E-07	0.188646	4.32E-06
D'	4.61E-08	3.93E-11	5.46E-08	1.67E-09
B"	0.189605	Held Constant	0.18962	4.39E-06
D"	4.62E-08	Held Constant	6.59E-08	1.71E-09

B'' and D'' are held constant in accordance with the findings of Hore *et al.* for computational purposes.

Table 2 presents the peak assignments and *J* values for the P and R branches of the $HCC^{35}Cl$ $2\nu_1$ and $\nu_1+\nu_2+2\nu_4$ bands.

Table 2

Observed lines and rotational assignments for cold bands of $HCC^{35}Cl$.

	$2\nu_1$		$\nu_1+\nu_2+2\nu_4$	
J	P(J)	R(J)	P(J)	R(J)
1			6600.5088	
2			6600.1281	6602.0229
3	6568.3570		6599.7438	6602.4007
4	6567.9702		6599.3558	6602.7687
5	6567.5813	6572.1411	6598.9670	6603.1381
6	6567.1894	6572.5107	6598.5754	6603.5057
7	6566.7980	6572.8813	6598.1833	6603.8712
8	6566.4031	6573.2418	6597.7881	6604.2352
9	6566.0093	6573.6089	6597.3916	6604.5968
10	6565.6139	6573.9717	6596.9950	6604.9560
11	6565.2139	6574.3334	6596.5934	6605.3146
12	6564.8135	6574.6934	6596.1907	6605.6699
13	6564.4116	6575.0512	6595.7866	6606.0243
14	6564.0081	6575.4079	6595.3802	6606.3763
15	6563.6033	6575.7621	6594.9723	6606.7261
16	6563.1967	6576.1155	6594.5624	6607.0746
17	6562.7885	6576.4671	6594.1506	6607.4210
18	6562.3788	6576.8169	6593.7370	6607.7658
19	6561.9673	6577.1652	6593.3212	6608.1076
20	6561.5543	6577.5118	6592.9037	6608.4483
21	6561.1398	6577.8568	6592.4839	6608.7866
22	6560.7235	6578.1997	6592.0628	6609.1233
23	6560.3059	6578.5416	6591.6401	6609.4580
24	6559.8860	6578.8818	6591.2147	6609.7906
25	6559.4660	6579.2201	6590.7878	6610.1214
26	6559.0433	6579.5568	6590.3587	6610.4504
27	6558.6188	6579.8918	6589.9283	6610.7772
28	6558.1931	6580.2256		6611.1021
29	6557.7660	6580.5569		6611.4253
30	6557.3372	6580.8873		6611.7468
31	6556.9066	6581.2158		6612.0670
32	6556.4746	6581.5432		6612.3824
33	6556.0409	6581.8684		6612.6985
34	6555.6057	6582.1913		6613.0125
35	6555.1690	6582.5130		6613.3243
36	6554.7305	6582.8333		6613.6336
37	6554.2905	6583.1517		6613.9434
38	6553.8491	6583.4688		6614.2501
39	6553.4056	6583.7839		6614.5528
40	6552.9613	6584.0974		6614.8561
41	6552.5152	6584.4094		6615.1576
42	6552.0673	6584.7200		6615.4573
43	6551.6179	6585.0280		6615.7555
44	6551.1671	6585.3351		6616.0523
45	6550.7146	6585.6404		6616.3480
46	6550.2602	6585.9442		6616.6428
47	6549.8050	6586.2459		
48	6549.3476	6586.5460		
49	6548.8888	6586.8449		
50	6548.4294	6587.1416		
51	6547.9670	6587.4366		
52	6547.5033	6587.7310		
53	6547.0384	6588.0222		
54	6546.5718	6588.3124		
55	6546.1032	6588.6009		
56	6545.6349	6588.8880		
57	6545.1622	6589.1726		
58	6544.6908			
59	6544.2157			
60	6543.7399			
61	6543.2617			
62	6542.7837			

HCC^{37}Cl $2\nu_1$ Band

Modeling the HCC^{37}Cl $2\nu_1$ band resulted in large differences between the observed and calculated, or residual, line positions in the region of J=30. Due to a characteristic pattern in the residuals when plotted as a function of J, a perturbation occurring from a Fermi resonance was suspected. Such perturbations arise from the internal transfer of energy between two closely spaced energy states which have the same vibrational symmetry. Bernath details how such perturbations may be modeled using a 2x2 Hamiltonian matrix where ΔE is the difference between the energies of the two states involved in the perturbation:

$$\Delta E = E_2^0 - E_1^0.$$

Note that the energies and difference in energy correspond directly to wavelengths and differences in wavelengths. A Hamiltonian matrix, H, may be used to model the perturbation where V is a term which describes the interaction between the two states:

$$H = \begin{bmatrix} E_1^0 & V \\ V & E_1^0 \end{bmatrix}$$

The Hamiltonian H has the eigenvalues:

$$E = \frac{E_1^0 + E_2^0}{2} \pm \frac{((E_1^0 - E_2^0)^2 + 4V^2)^{1/2}}{2}$$

Which may be expanded to:

$$E_{\pm} = \frac{E_1^0 + E_2^0}{2} \pm \Delta E \left(1 + 4\frac{V^2}{2(\Delta E)^2} + \frac{(\frac{1}{2})(-\frac{1}{2})}{2!}\left(\frac{4V^2}{\Delta E^2}\right)^2 + \cdots \right) \Big/ 2$$

Which gives the energies or wavelength of the perturbed states in terms of the zeroth order energies E_1^0 and E_2^0 and V:

$$E_1 = E_- = E_1^0 + \frac{-V^2}{\Delta E} + \frac{V^4}{\Delta E^3} + higher\ order\ terms$$

$$E_2 = E_+ = E_2^0 + \frac{V^2}{\Delta E} - \frac{V^4}{\Delta E^3} + higher\ order\ terms$$

The contribution of the $\frac{V^4}{\Delta E^3}$ term and higher order terms is expected to be negligible, resulting in the approximation:

$$E_1 = E_1^0 + \frac{-V^2}{\Delta E}$$

$$E_2 = E_2^0 + \frac{V^2}{\Delta E}$$

In order to model more than one perturbation larger matrices are required. The $HCC^{37}Cl$ $2\nu_1$ band contains two perturbations that we detected and thus required a 3x3 Hamiltonian with terms V_{01} and V_{02} characterizing the perturbations for each transition from the zeroth order state to the first and second order states respectively. $V_{12} = 0$ by computational necessity:

$$H = \begin{bmatrix} E_0^0 & V_{01} & V_{02} \\ V_{01} & E_1^0 & V_{12} \\ V_{02} & V_{12} & E_2^0 \end{bmatrix}$$

The algebra required to expand and solve the above Hamiltonian for *n* terms E_n follows the same form as the 2x2 example but is more complicated.

By fitting the residuals of the measured and modeled $HCC^{37}Cl$ $2\nu_1$ band peaks, V_{01} and V_{02} may be obtained along with ΔG which is the difference in vibrational energy between the band modeled with and without the perturbations considered, ΔG_1

and ΔG_2 which are the respective discrepancies of vibrational energy from the 1st and 2nd perturbed states to the visible state, and ΔB_1 and ΔB_2 which are the respective differences in the rotational constants of the unseen states and the visible state. Table 3 presents these constants, which are related to the 3x3 Hamiltonian matrix elements as follows:

$$E_0^0 = G + BJ(J+1) \ldots$$

$$E_1^0 = G_1 + (B + \Delta B_1)J(J+1) \ldots$$

$$E_2^0 = G_2 + (B + \Delta B_2)J(J+1) \ldots$$

Table 3

Calculated constants for $HCC^{37}Cl$ $2v1$ cold band.

$2v_1$		
Constant	Value	Uncertainty
ΔG	-5.15E-05	1.37E-04
ΔG_1	-1.76418	3.74E-02
ΔG_2	-3.05	7.39E-02
ΔB_1	0.00215112	4.63E-05
ΔB_2	2.39E-03	6.05E-05
V_{01}	0.0257695	0.00120767
V_{02}	0.0465844	0.00125227

While this perturbation was modeled as a Fermi-type resonance, the possibility that it is a 2nd-order Coriolis resonance cannot be excluded without further analysis, which may be an avenue for future work.

Table 4 presents peak assignments and *J* values for the $HCC^{37}Cl$ $2v_1$ band as modeled with the double perturbation and confirmed via the method of combination differences. Accuracy was typically 2.4×10^{-4} cm^{-1}.

Table 4

Observed lines and rotational assignments for $2\nu_1$ cold band of $HCC^{37}Cl$

$2\nu_1$					
J	P(J)	R(J)	J	P(J)	R(J)
0	6569.8143		34	6556.251	6581.8869
1	6569.4414	6570.5583	35		
2	6569.0649		36		6582.4912
3	6568.6884	6571.2903	37		6582.8113
4	6568.3104	6571.6559	38		6583.1243
5		6572.0196	39		6583.4349
6	6567.5521	6572.3823	40	6553.6557	6583.7436
7	6567.1668	6572.7427	41	6553.2207	6584.0502
8	6566.7822	6573.1024	42	6552.7836	6584.3554
9		6573.4596	43	6552.3456	6584.6585
10		6573.8154	44	6551.9060	6584.9595
11		6574.1701	45	6551.4641	6585.2596
12	6565.2286	6574.5227	46	6551.0214	6585.5573
13	6564.8373	6574.8740	47	6550.5766	6585.8550
14	6564.4440	6575.2235	48	6550.1300	6586.1484
15	6564.0482		49		6586.4401
16	6563.6516	6575.9162	50	6549.2324	6586.7337
17	6563.2530	6576.2623	51	6548.7812	6587.0233
18	6562.8532	6576.6056	52	6548.3288	6587.3075
19	6562.4520	6576.9471	53	6547.8758	6587.5993
20	6562.0490	6577.2874	54	6547.4200	6587.8827
21	6561.6441	6577.6257	55	6546.9634	6588.1719
22	6561.2381	6577.9628	56	6546.5045	6588.4490
23	6560.8306	6578.2982	57		6588.7294
24	6560.4217	6578.6324	58	6545.5846	6589.0084
25	6560.0113	6578.9647	59	6545.1187	6589.2846
26	6559.5996	6579.2957	60	6544.6551	6589.5586
27	6559.1879	6579.6266	61	6544.1878	6589.8337
28	6558.7317	6579.9689	62	6543.7220	6590.1031
28	6558.7881	6579.9107	63		
29	6558.3461	6580.2704	64		6590.6419
30	6557.9306	6580.5969	65		6590.9070
31	6557.5120	6580.9210	66		6591.1734
32	6557.0912	6581.2443	67		6591.4369
33	6556.6709	6581.5640			

Unassigned value of *J* are from overlapped peaks or peaks that could not be found accurately. All units are in cm^{-1}.

Figure 11 shows the residuals of the observed and calculated line positions for the $HCC^{37}Cl$ $2\nu_1$ band plotted against *J* along with the fit of the residuals.

Figure 12 shows the residuals of the observed and calculated line positions for the $HCC^{35}Cl$ $2\nu_1$ band, which does not contain a perturbation, plotted against J.

Note that while the residuals in Figure 12 are randomly distributed and therefore may be attributed to experimental noise, limitation in the Voigt line shaping, and other random errors, the residuals in Figure 11 have a distinct pattern caused by the perturbation. The divergence in the values of the residuals with one tail increasing in

value and one tail decreasing in value is a characteristic pattern of a single perturbation while the additional points in between the diverging tails is characteristic of a double perturbation.

Figure 11: Residuals with perturbation pattern and fit for the $HCC^{37}Cl$ $2v_1$ band.

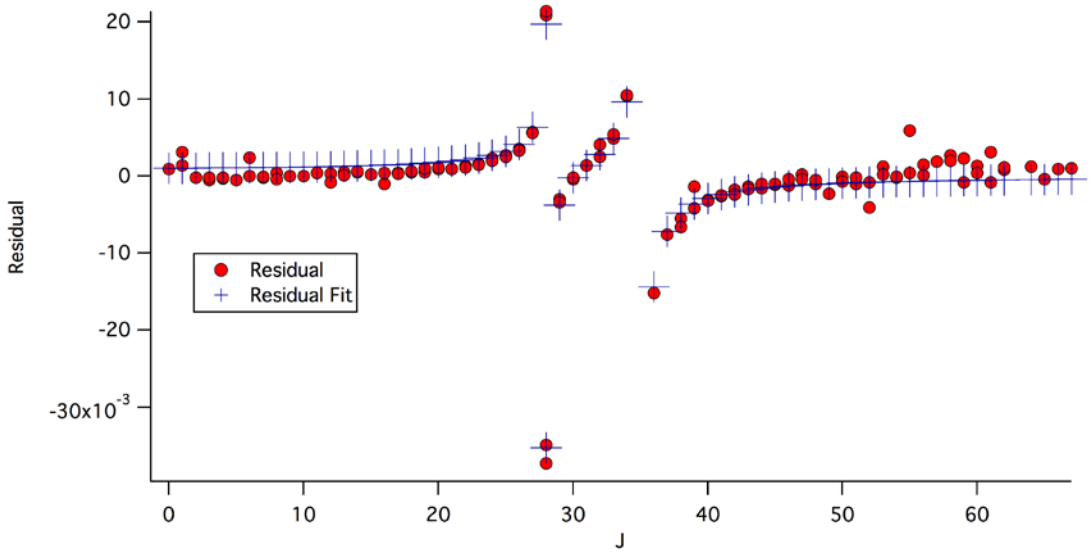

Figure 12: Residuals for the $HCC^{35}Cl$ $2v_1$ band.

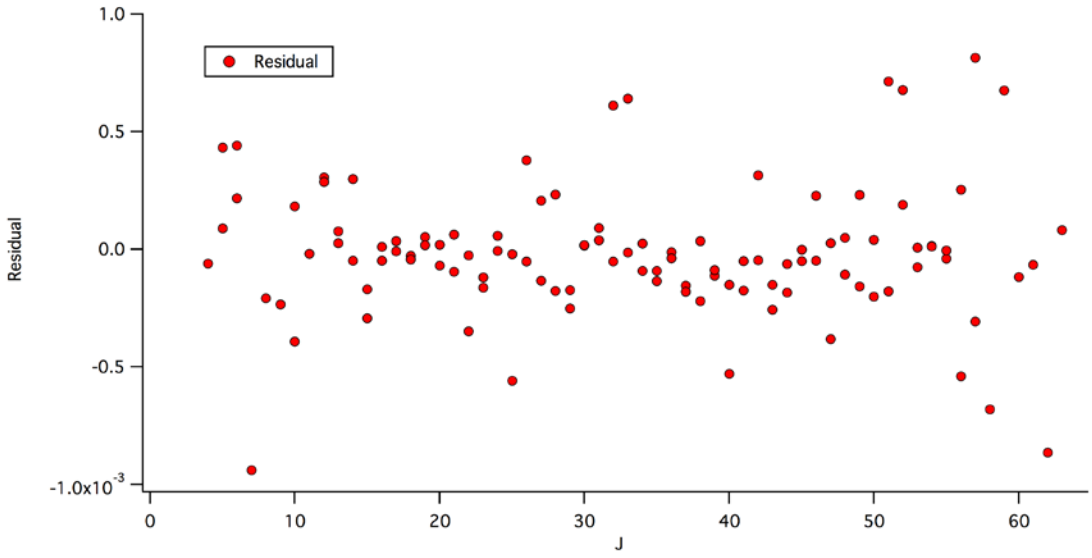

Hot Band

The $HCC^{35}Cl$ $(\nu_1+\nu_4)^1$-$\nu_4{}^1$ hot band showed *l*-type doubling that caused the observed peaks to vary in their spacing across the wavenumber scale; in some portions the doublets would overlap and be indistinguishable from a single peak. As suggested by Yu *et al*., splitting of the peaks can be modeled by:

$$\Delta\nu = qJ(J+1) + q_D\big(J(J+1)\big)^2$$

Where $\Delta\nu$ is the distance between the peaks of the doublet, *q* and qD are the *l*-type doubling constants. As *q* and *qD* are shown to be non-zero for both the upper and lower states, both states must be π-states.

Table 5 presents calculated constants for the $HCC^{35}Cl$ hot band.

Table 5

Calculated constants for HCC35Cl $(\nu_1+\nu_4)1$-$\nu_4{}^1$ hot band.

$2\nu_1$		
Constant	Value	Uncertainty
Nu0	6529.99	4.77E-04
B'	0.188894	7.52E-06
D'	8.45E-09	7.49E-10
q'	-0.000160104	5.06E-06
qD'	-7.35E-09	7.65E-10
B"	0.189707	7.56E-06
D"	1.96E-08	1.44E-09
q"	-0.000127256	4.93E-06
qD"	-2.97E-09	5.96E-10

Table 6 presents peak assignments and *J* values for the $HCC^{35}Cl$ $(\nu_1+\nu_4)^1$-$\nu_4{}^1$ hot band modeled as a series of doublets. Our assignment of the $(\nu_1+\nu_4)^1$-$\nu_4{}^1$ band was confirmed via the method of combination differences using the assignments of Nela *et al*. Accuracy was typically $1.8\text{x}10^{-3}$ cm^{-1}.

Table 6

Observed lines and rotational assignments for the $(v_1+v_4)^1$-v_4^1 hot band of $HCC^{35}Cl$.

$(v_1+v_4)^1$-v_4^1					
J	P(J)	R(J)	J	P(J)	R(J)
3	6528.4603		19	6522.0922	
3	6528.4604		19	6522.0925	
4	6528.0720		20	6521.6804	6537.2238
4	6528.0720		20	6521.6802	6537.2472
5	6527.6856		21	6521.2721	6537.5687
5	6527.6856		21	6521.2624	6537.5948
6	6527.2956		22	6520.8570	6537.9103
6	6527.2956		22	6520.8496	6537.9377
7	6526.9047	6532.5954	23	6520.4404	6538.2512
7	6526.9047	6532.5954	23	6520.4313	6538.2817
8	6526.5128	6532.9632	24	6520.0272	6538.5919
8	6526.5128	6532.9632	24	6520.0114	6538.6235
9	6526.1193	6533.3283	25	6519.6082	6538.9286
9	6526.1193	6533.3283	25	6519.5905	6538.9642
10	6525.7235	6533.6912	26	6519.1892	6539.2653
10	6525.7235	6533.6912	26	6519.1694	6539.3023
11	6525.3262	6534.0543	27	6518.7683	
11	6525.3261	6534.0543	27	6518.7463	
12	6524.9272	6534.4116	28	6518.3451	
12	6524.9269	6534.4116	28	6518.3196	
13	6524.5263	6534.7692	29	6517.9204	
13	6524.5263	6534.7707	29	6517.8944	
14	6524.1265	6535.1281	30	6517.4947	
14	6524.1265	6535.1290	30	6517.4661	
15		6535.4796	31	6517.0671	
15		6535.4875	31	6517.0363	
16	6523.3178	6535.8319	32	6516.6378	
16	6523.3178	6535.8452	32	6516.6057	
17	6522.9103	6536.1809	33	6516.2079	
17	6522.9103	6536.1953	33	6516.1737	
18	6522.5020	6536.5316	34	6515.7765	
18	6522.502		34	6515.7439	
			35	6515.3428	
			35	6515.3080	
			36	6514.9121	
			36		

Unassigned value of *J* are from overlapped peaks or peaks that could not be found accurately. All units are in cm^{-1}.

Discussion

This work extends the assignments of Nela *et al*. in the $2\nu_1$ bands for $HCC^{35}Cl$ and $HCC^{37}Cl$ and the $\nu_1+\nu_2+2\nu_4$ band for $HCC^{35}Cl$. We have assigned a previously unreported $(\nu_1+\nu_4)^1$-ν_4^1 hot band for $HCC^{35}Cl$. We have obtained accuracies for unblended line assignments as good as $2.5\text{x}10^{-4}$ cm^{-1} which surpasses previous work in this region by an order of magnitude. This level of accuracy was enabled by using a high-sampling rate, non-multiplexed analog to digital converter for data collection along with processing out background noise and performing baseline correction using a novel fast-Fourier transform-based technique along with signal averaging of multiple spectra.

Background noise and signal baseline irregularities are a general problem for spectroscopy and are particularly difficult factors to control outside of the laboratory. Our fast-Fourier transform-based method is capable of removing background noise and irregularities for each scan conducted without the need for a calibration or blank scan or other external data points. This offers the possibility of incorporating automatic data processing to expand the capabilities of spectrometers used in practical applications such as environmental analysis that face a wide range of experimental conditions, often without the benefit of expert users or field-serviceability.

Our resolution allowed the identification of *l*-type splitting with $\Delta\nu$ values ranging from complete overlap to $3.5\text{x}10^{-2}$ cm^{-1} in the $(\nu_1+\nu_4)^1$-ν_4^1 hot band of $HCC^{35}Cl$. π upper and lower states required a second order model to correctly characterize the splitting.

The use of Voigt line shaping to reconstruct the dominant $2\nu_1$ band of $HCC^{35}Cl$ allowed the subtraction of that band from the original spectrum, revealing previously blended or indeterminate peaks of the $2\nu_1$ band of $HCC^{37}Cl$. The same technique may be applied to reveal and allow the characterization of other $HCC^{37}Cl$ bands. This ability is particularly useful in light of the lack of commercial availability of isotopically pure 1,2-dichloro(^{37}Cl)ethylene, meaning that without performing a synthesis from available forms of ^{37}Cl, the spectrum of $HCC^{37}Cl$ must practically be observed in the presence of a higher concentration of $HCC^{35}Cl$.

We have identified a double perturbation in the $2\nu_1$ band of $HCC^{37}Cl$ and obtained constants characterizing the two hidden energy states involved in the perturbation through the use of a 3x3 Hamiltonian approximation.

Our laser pyrolysis method, adapted from the work of Hore *et al*., can safely generate low pressures of monochloroacetylene, which generally must be made *in situ* due to its explosive and extremely reactive nature. Within the spectral range which we examined, no significant impurities interfered with our analysis; the only contaminant clearly evident was trace acetylene. This success suggests that other halogenated derivatives of acetylene may be generated using a similar procedure.

Glossary

"*As a function of*"*:* For the statement "Y as a function of X" a graph is constructed which plots the X values along the horizontal axis and the Y values along vertical axis. This is typically intended to allow the examination of a Y value (such as absorbance) at any value of X (such as wavenumber).

Band: A collection of spectral peaks corresponding to a particular collection of rotational and vibrational transitions.

Band Origin: The center of a band, where J=0.

Δv*:* The spacing in between any adjacent peaks of the same band. May be given interchangeably in terms of frequency or energy.

Fast-Fourier transform (FFT): a computational mathematical method that changes the domain of a set of data. Time-domain data is often converted to the frequency-domain or vise-versa.

Frequency domain: Data in the frequency domain is data for which any given data point is associated with a defined frequency of electromagnetic radiation. Frequency domain data is either obtained from experiments where the detector is capable of measuring the data in terms of frequency, or more commonly computationally obtained from data in the time domain. Frequency domain may be used to refer to data that is strictly in the wavenumber domain, since the former may be converted facilely to the latter by taking the reciprocal.

Frequency: The number of times per second that an electromagnetic wave oscillates, typically defined in cycles per second, which is equivalent to inverse seconds or Hertz (Hz). Higher frequency light contains more energetic photons.

Ground state: The lowest quantum energy level possible for a particular form of energy, *e.g.* rotational, vibrational, electronic.

J-Value or J: The rotational quantum number that indicates at which quantized energy level a molecule is rotating. In a rotational-vibrational band *J* increases by 1 with each successive peak outward from the band origin.

Igor Pro: A computer program that can be used to record signals from detectors and instruments, analyze data, and create graphs of data.

Isotope: An atom which has a particular number of neutrons in its nucleus. Many atoms have different isotopes which have slightly different masses but very similar chemical behavior. ^{35}Cl and ^{37}Cl are the most common isotopes of chlorine and each contain a combination of protons and neutrons summing to 35 and 37, respectively.

Isotopologue: A pair of molecules that differ only in the isotopic composition of their atoms. $HCC^{35}Cl$ and $HCC^{37}Cl$ are isotopologues.

Laser table: A metal table with threaded inserts for locating and securing equipment. Often isolated from structural vibrations which may interfere with the equipment.

Monochloroacetylene: a compound consisting of two carbon atoms triple bonded to each other, with one bonded to a hydrogen atom and the other bonded to a chlorine atom. Note that chlorine occurs predominantly in two isotopes.

Photon: A fundamental particle that forms the basis for all electromagnetic radiation, including visible and infrared light. While photons are particles, they travel with the properties of a wave.

Perturbation: A deviation from expected spectral line positions or other behavior that requires additional modeling and explanation.

Quantum: One unit of quantized energy, defined by a specific quantum number. Plural: Quanta.

Quantized: Only able to adopt specific, stepwise values of energy. Energy values between the quantized steps are not possible.

Quantum Number: A unitless number which defines a quantized energy level or other quantum behavior.

Rotational constant: a physical constant based on spectroscopic analysis of the rotational energy transitions of a compound that is inversely related to the moment of inertia.

Schlenk Line: An apparatus also known as a dual-manifold. Two systems of glass tubing connected via valves such that gases or vacuum may be routed into and out of connected vessels. Typically connected to a strong vacuum pump to allow evacuation of the manifolds and of connected vessels to ensure purity of whatever gases are being used.

Spectroscopy: The study of compounds through their characteristic patterns of absorption or release of a defined kind of electromagnetic radiation.

Time domain: Data in the time domain is data for which any given data point is associated with a defined point in time. Generally obtained from experiments where data collection takes place over a period of time.

Torr: a unit of pressure corresponding to $1/760^{th}$ of a standard atmosphere (atm). Thus, 760 torr is approximately the pressure experienced at sea level on earth. A *millitorr* is $1/1000^{th}$ of one torr.

Tunable diode laser: A laser which is capable of operating at a large number of wavelengths, typically in a smooth scan between two defined wavelengths.

Wavelength: A physical property of electromagnetic radiation, common defined in nanometers (nm), that corresponds to distance between two consecutive peaks of the electromagnetic wave. More generally, a measurement used to define a specific color of light. For example, visible light ranges from 400 to 700 nm. Lower wavelength light contains more energetic photons.

Wavenumber: The number of cycles per a defined distance that an electromagnetic wave oscillates. It may be obtained by taking the reciprocal of wavelength. Typically specified in inverse centimeters (cm^{-1}).

Bibliography

Bernath, Peter F. *Spectra of Atoms and Molecules*. New York: Oxford UP, 1995. Print. Topics in Physical Chemistry Ser.

Demtröder, W. *Molecular Physics : Theoretical Principles and Experimental Methods*. Weinheim: Wiley-VCH, 2005. Print.

Dougherty, R C, and H. Collazo-Lopez. "Reduction of Organochlorine Emissions from Municipal and Hazardous Waste Incinerators." *Environmental Science & Technology* 21.6 (1987): 602-4. Web.

Hardwick, J.L., Martin, Z.T., Schoene, E.A., Tyng, V., and Wolf, E.N. "Diode Laser Absorption Spectrum of Cold Bands of C 2HD at 6500 Cm −1." *Journal of Molecular Spectroscopy* 239.2 (2006): 208-15.

Herzberg, Gerhard. *Molecular Spectra and Molecular Structure*. 2d ed. New York: Van Nostrand, 1950. Print. Prentice-Hall Physics Ser.

Hore, Russell, and Wesendrup. "High-Resolution Tunable Diode Laser Study of the *v*2 Band System of Monochloroacetylene." *Journal of Molecular Spectroscopy* 213.2 (2002): 153-57.

Madej, Alan A., A. John Alcock, Andrzej Czajkowski, John E. Bernard, and Sergei Chepurov. "Accurate Absolute Reference Frequencies from 1511 to 1545 Nm of the *v*1+*v*3 Band of 12 C2H2 Determined with Laser Frequency Comb Interval Measurements." *Journal of the Optical Society of America B* 23.10 (2006): 2200.

Nela, Niskanen, Vaittinen, Halonen, Burger, and Polanz. "High-resolution Infrared and Laser Photoacoustic Spectroscopy of Monochloroacetylene." *Molecular Physics* 100.5 (2002): 655-65.

Saarinen, Maria, Halonen, Lauri, and Polanz, Oliver. "High-resolution Photoacoustic Overtone Spectrum of Monochloroacetylene Using a Titanium: Sapphire Ring Laser Spectrometer." *Chemical Physics Letters* 219.3 (1994): 181-86.

Yu, Shanshan, Alireza Shayesteh, and Peter F Bernath. "The Vibration-rotation Emission Spectra of Gaseous CdH2 and CdD2." *The Journal of Chemical Physics* 122.19 (2005): 194301.